Article

Occurrence Modes of AAEMs (Na$^+$ and Ca^{2+}) and the Effect on the Molecular Structures of Zhundong Coal via Quantum Chemistry

Xiaoling Wang, Shaoqing Wang,* Yungang Zhao, Ruifeng Mu, and Yan Shao

Read Online

ACCESS | Metrics & More | Article Recommendations | SI Supporting Information

ABSTRACT: Zhundong coal is known for its high content of alkali and alkaline earth metals (AAEMs), which greatly influences coal processing and utilization. To reveal the occurrence modes and the effect of AAEM ions on the molecular structures of Zhundong coal, the previously constructed molecular structure models of vitrinite-rich and inertinite-rich Zhundong coal (ZD-V and ZD-I) were selected to simulate using quantum chemical methods. By focusing on Na$^+$ and Ca^{2+}, the adsorption capacity at different adsorption sites was investigated based on the density functional theory (DFT), and the effects of adsorption of Na$^+$ and Ca^{2+} on nearby atomic charges, chemical bonds, and molecular orbitals were investigated. Results show that compared with ZD-I, ZD-V contains a more negative electrostatic potential (ESP) distribution and lower bond order, indicating that vitrinite contains more adsorption sites for AAEM ions and exhibits stronger chemical reactivity. Na$^+$ and Ca^{2+} are easily adsorbed to the most negative ESP with the optimal adsorption site near the carbonyl group (C=O). Compared with adsorbed Na$^+$, Ca^{2+} has a smaller adsorption distance from the molecule and a higher adsorption energy. Ca^{2+} can transfer more charge than Na$^+$ and has more affinity with the coal molecule. Ca^{2+} at all adsorption sites is bound to organic molecules by chemisorption, which also reveals the reason for the low water-soluble Ca content in coal at the molecular level. Adsorption of AAEM ions has a more significant effect on the chemical bond of oxygen-containing functional groups near AAEM ions compared to the overall molecular fragments, which makes the nearby chemical bonds (C−O/C=O) decrease in bond order and increase in bond length. Ca^{2+} makes the nearby chemical bonds more prone to break than Na$^+$. Additionally, Ca^{2+} has a more significant impact on the energy gaps (ΔE_{gap}) compared to Na$^+$. Adsorption of Ca^{2+} near the carbonyl and carboxyl groups leads to a significant decrease in ΔE_{gap}, indicating an enhanced chemical reactivity of coal molecular fragments.

1. INTRODUCTION

Zhundong coal field has a large amount of resources with coal reserves of about 390 billion tons and has become the largest intact coalfield in China.[1] The most prominent feature of Zhundong coal is the presence of significant amounts of alkali and alkaline earth metals (AAEMs),[2,3] which was associated with the carboxylic and phenolic functionalities in the coal structure.[4,5] On the one hand, the inherent AAEMs may cause severe fouling, corrosion, and slagging problems during coal gasification or combustion.[6,7] On the other hand, AAEMs play an exceedingly essential role in the thermal conversion and utilization of coal, which can be used as inherent catalysts to participate in the subsequent char gasification or combustion reactions.[8−10] These effects are related to the occurrence modes of AAEMs in coal.

From the perspective of coal utilization, Zhundong coal is a typical high volatile with low-rank coal, which is regarded as high-quality coal for clean coal technology such as coal liquefaction and gasification, and the thermal reactivity of coal is related to its chemical structure. In the past decades, with the comprehensive utilization of various advanced techniques,

considerable information regarding the chemical structure of coal has been obtained by solid-state ^{13}C nuclear magnetic resonance,[11,12] Fourier transform infrared spectroscopy,[13,14] high-resolution transmission electron microscopy,[15−17] X-ray photoelectron spectroscopy,[15,18] and X-ray diffraction.[14,19] Based on these structural parameters, a macromolecular structure model of coal can be constructed and used to explore the mechanism of coal pyrolysis. Wang et al.[20] used the previous molecular model for vitrinite and inertinite of Heidaigou coal to calculate the bond order and bond length distribution via quantum chemical calculation, respectively, and evaluated the thermal reactivity of Heidaigou coal. Zhao et al.[21] calculated a sequence of electronic property parameters of

thermally altered coals, including bond order, bond length, atom charge, and molecular orbitals, which are extremely helpful for predicting the structural reactivity of thermally altered coals. Pan et al.[22] unraveled the chemical behavior of kerogen from the perspective of electronic properties, providing an insight on the influence and mechanism of heteroatoms containing organic oxygen, nitrogen, and sulfur on the kerogen molecular structure. However, the electronic properties of the molecules of Zhundong coal are less studied in quantum chemistry.

On the other hand, considering the enrichment of AAEM in Zhundong coal, it plays an important role in the structural reactivity of Zhundong coal molecules. Occurrence modes and contents of AAEM in the Zhundong coal are mainly determined by the sequential extraction method, which is mainly divided into water-soluble, exchangeable, acid-soluble, and insoluble AAEM.[23] Bai et al.[24] studied the occurrence modes of sodium in Zhundong coal and found that water-soluble, especially hydrated ion, was the dominant form of sodium. The improved sequential extraction method was proposed by Yang et al.[25] to study the occurrence modes of AAEM with Zhundong coal. The results revealed that Na is mainly water-soluble, which is halite or in the form of surface-bound Na^+, whereas Ca is mainly acid-soluble, which is in the form of carbonates together with a small number of sulfates. It is worth noting that Ca in Zhundong coal is mainly present as ammonium acetate-soluble form, which is easily bound to organic matter and occurs in the form of calcium carboxylate, in addition to being associated with inorganic minerals.[26−28] Although the occurrence modes of AAEM in coal are given from experimental perspectives, the detailed location between AAEM and coal macromolecular structures, distribution patterns, and organic affinities with elements are hard to obtain at experimental levels. At present, with the continuous development of molecular simulation technology, this issue is well solved by using density functional theory (DFT). DFT can also quantify the microscopic adsorption capacity of organic matter binding to metal ions in coal.[29,30] Sun et al.[29] calculated the electrostatic potential (ESP) distribution in coal molecules with the aid of DFT to determine the optimal adsorption sites of alkali metals in coal and build AAEM occurrence models in the quantification and visualization in high-alkali coal. Limited by the computational power of DFT, it is hard to calculate and assess the effect of AAEM on the macromolecule structure. Consequently, Jeong et al.[31] selected a representative molecular fragment and investigated the influence of AAEMs on the bond breaking mechanism of lignin model compounds at the molecular level through extensive DFT study (including bond order and bond length calculation). Therefore, if the representative small molecule fragments are well selected from coal macromolecules to study the occurrence modes of AAEM and its effect on the molecular structure, it will be more practical.

Dai et al.[32] also point out that the specific position and/or structure of the nonmineral elements' host in coal is a key issue to further evaluate more fully the modes of occurrence. At the same time, how AAEM affects the coal matrix cannot be observed at the atomic level by experimental means alone. A good case is that it is not sufficient to understand the occurrence modes of AAEM in Zhundong coals by categorizing the AAEM elements according to their solubility. These issues restrict the development of studying the effect of AAEM on the thermochemical conversion process of coal and

its precise reaction mechanism. Considering that the bonding ability between AAEM ions and coal molecules in Zhundong coal is not clear, different sites of AAEM ion binding to coal molecules also have a differential effect on the structure of coal molecules, which, in turn, affects their reaction behavior. Here, the binding ability can be quantified in terms of the adsorption energy and degree of charge transfer, and the reactivity evaluation is considered in terms of effects on bond order, bond length, and molecular orbitals. Therefore, revealing the electronic properties of coal molecules from a quantum chemical perspective is critical for predicting the structural reactivity of Zhundong coal-containing AAEM systems. So, in this study, in addition to identifying the optimal binding sites to coal molecular fragments, the main purpose aims to investigate the effects of the adsorption of Na^+ and Ca^{2+} at different binding sites on the electronic properties of coal molecular fragments, including atomic charges, chemical bonds, and molecular orbitals, trying to reveal the mechanism of the special reactivity of high-AAEM coal from a quantum chemical perspective.

2. METHOD

2.1. Quantification of AAEMs. AAEMs in coal can be categorized into water-soluble, exchangeable, acid-soluble, and insoluble forms based on their solubility and reactivity properties.[24,25] Water-soluble AAEMs can be dissolved and leached out by water. Exchangeable AAEMs in coal are loosely bound to the coal matrix (e.g., sodium carboxylate and calcium carboxylate) and can be easily exchanged with other substances. These metals can be released through ion exchange processes. Acid-soluble AAEM is a metal that can be dissolved by strong acids. Insoluble AAEMs are metals that do not dissolve significantly in water or strong acids, which are typically associated with mineral matter such as clays and silicates in coal.

To quantify the occurrence and content of AAEM in Zhundong coal, sequential extraction experiments were conducted. Deionized water, ammonium acetate (1.0 mol/L CH_3COONH_4), and hydrochloric acid (1.0 mol/L HCl) were used to sequentially extract coal samples for 24 h at 60 °C with a solid to liquid ratio of 1 g to 50 mL. The content of AAEM was determined by inductively coupled plasma-optical emission spectroscopy (ICP-OES). Total contents of AAEMs were converted to coal weight base, and contents of AAEMs in the four occurrence modes are normalized by dividing the total AAEM content, as shown in Table 1. Compared with K and Mg, the total content of Na and Ca is relatively enriched,

Table 1. Occurrence Modes and Contents of AAEMs in the Zhundong Coals

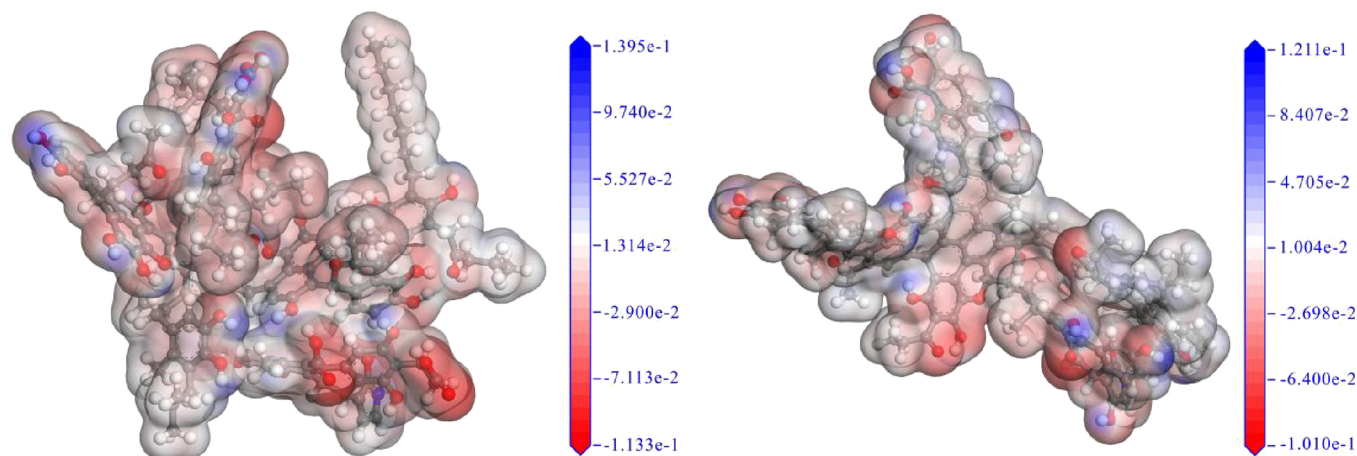| samples	AAEM	content/wt %				
		water-soluble	exchangeable	acid-soluble	insoluble	total content
ZD-V	Na	64.16	30.94	3.98	0.92	0.22
	Ca	0.77	70.13	28.34	0.76	0.40
	K	27.25	18.31	54.33	0.11	0.01
	Mg	1.90	18.89	78.55	0.66	0.15
ZD-I	Na	75.44	23.03	0.07	1.46	0.16
	Ca	0.22	81.30	14.52	3.96	0.66
	K	29.99	26.93	40.99	2.09	0.01
	Mg	0.26	9.97	84.20	5.58	0.23

Figure 1. ESP of the ZD-V and ZD-I macromolecular surface.

especially water-soluble and exchangeable, and the interaction with coal molecules is more significant. So, in this study, Na and Ca were chosen as representative AAEMs to simulate the interaction with coal molecules.

2.2. Modeling and Calculation Details. In our previous work, the chemical structure of two Zhundong coals with different enriched macerals (vitrinite, inertinite) was studied using ^{13}C NMR, XPS, and FTIR experiments, and the results showed significant variance in the structural composition at a molecular level for vitrinite-rich and inertinite-rich Zhundong coals. ZD-V is mostly composed of chain hydrocarbons, whereas ZD-I is dominated by cyclic hydrocarbons with linked aromatic rings. ZD-V contains more oxygen-containing functional groups than ZD-I, and the different types of oxygen-containing functional groups will have a great effect on the occurrence for AAEM ions in coal. Based on this, the molecular structure models were constructed, and more modeling construction details can be seen in our previous work.[33]

The final lowest energy models for the two Zhundong coals constructed were output to perform the next quantum chemical calculations. All computations following were carried out using DFT as implemented in the DMol^3 module on the Materials Studio software, including the adsorption energy, Mulliken charge, bond order, bond length, and molecular orbitals. Before the adsorption with AAEM ions was calculated, the ESP of Zhundong coal molecules was calculated to better determine the adsorption sites. Generalized gradient approximation (GGA) with Perdew–Burke–Ernzerhof (PBE) functional was adopted.[34] The DNP was used to describe the electronic basis set, and the Grimme method was used for DFT-D correction. Spin unrestricted was chosen.[35] Total self-consistent field (SCF) tolerance criteria, integration accuracy criteria, and orbital cutoff quality criteria were set at fine. Multipolar expansion was set at octupole. To simulate the real binding behavior between the AAEM ion and the coal molecule, the solvation effect was considered, and the conductor-like shield model (COSMO) with a permittivity of 78.54 (water) was selected. The convergence tolerance values for energy, maximum force, and maximum displacement were 1×10^{-5} Ha, 2×10^{-3} Ha/Å, and 5×10^{-3} Å, respectively. The geometric optimization of Zhundong coal molecular models together with Na$^+$ or Ca^{2+} was carried out, and adsorption energy analysis was performed to determine the binding capacity of coal molecules to AAEM ions. The adsorption energy for various adsorption sites between the two coal molecules with AAEM ions was calculated as follows:

$$\triangle E_{ads} = E_{coal-ions} - (E_{coal} + E_{ions}) \tag{1}$$

where $E_{coal-ions}$ is the total binding energy for the adsorption complex, E_{coal} is the total energy of the adsorbent, and E_{ions} is the total energy of the adsorbate. The absolute value of the adsorption energy is related to the adsorption capacity.

3. RESULTS AND DISCUSSION

3.1. Electrostatic Potential (ESP) Analysis. Molecular ESP gives an indication of the net electrostatic effect produced by the total charge distribution (electron + nuclei) of the molecule, which correlates with dipole moments, electronegativity, partial charges, and chemical reactivity of the molecules.[36] The positive and negative ESP of the molecular regions was described by the isopotential surface, which can provide a visual insight into the relative polarity of the molecules. The different values of ESP at the surface are represented by different colors, and the ESP increases in the order are red < white < blue. Figure 1 provides visual insight into the chemical active sites and comparative reactivity of atoms in the molecular models of ZD-V and ZD-I. There are notable differences in the distribution of ESP between these different macerals. Compared with ZD-I, ZD-V contains more negative potential distribution. The maximum negative potential of ZD-V is $1.133e^{-1}$ au, which is slightly larger than that of ZD-I ($1.010e^{-1}$ au), indicating that the molecular structure of vitrinite-rich coal contains more chemically reactive sites. Several negative potential regions of Zhundong coal molecules are concentrated near oxygen-containing functional groups, which are related to the lone pair electrons of oxygen atoms.[37] The overlap region between the carbonyl oxygen and a single benzene ring shows the strongest electrophilicity. Negative potential regions are also found near ether-bonded oxygen, alcohol hydroxyl oxygen, and phenol hydroxyl oxygen, indicating their potential as metal adsorption sites.[29] Additionally, negative potential regions are observed on either side of the benzene ring, corresponding to the π electron.

On the other hand, the maximum positive potential in ZD-V and ZD-I is 1.395 and $1.211e^{-1}$ au, respectively, which is related to the hydrogen atom in the molecule.[38] These positive potential regions are prominently distributed around hydrogen

in the carboxyl group, hydrogen in the phenol hydroxyl group, and hydrogen in the alcohol hydroxyl group. These locations serve as active sites for the nucleophilic reactions. In summary, the distribution of ESP in Zhundong coal provides valuable insights into the polarity and reactivity of the different molecular regions. Understanding these patterns is essential for comprehending the chemical behavior and potential utilization of the coal.

3.2. Bond Order Analysis. Figure 2 shows the distribution of bond order of all chemical bonds ranging from 0.5 to 1.3.
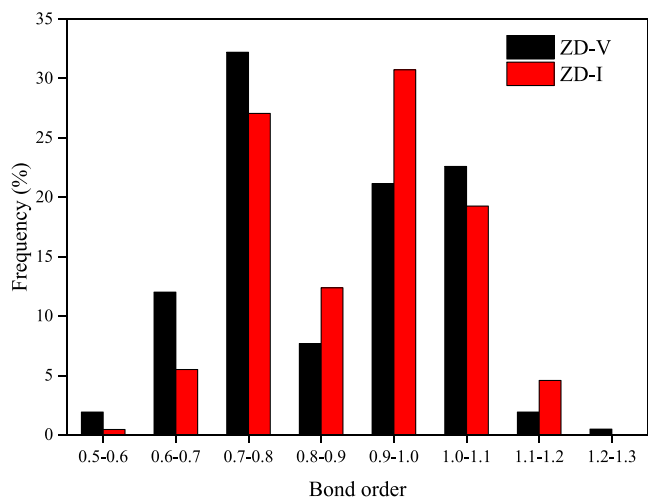
Figure 2. Distribution of bond orders for ZD-V and ZD-I.

Notably, ZD-I contains few bonds in the range of 0.5−0.6 and 0.6−0.7 bond order. These bonds are preferentially broken during pyrolysis or liquefaction. In other words, compared with vitrinite-rich coal, the pyrolysis performance of inertinite-rich coal is poor. ZD-V has a peak value in the range of 0.7−0.8 bond order, whereas ZD-V has a higher peak in the range of 0.9−1.0 bond order, both of which concentrated more than 30% of the total bond order. For bonds in the range of 1.1− 1.3, the ZD-I content is almost twice as much as the ZD-V content. In general, inertinite has numerous bonds with high bond order, whereas vitrinite has more bonds with low bond order. Therefore, vitrinite can break more bonds and shows higher reactivity than inertinite when coal is under heating, which is consistent with the results obtained from previous experimental studies.[39,40] To visually catch the easiest breaking band of ZD-V and ZD-I, a band order less than 0.7 was counted according to the results of quantum chemical simulation. Figure S1 shows the easiest breaking place of chemical bond for ZD-V and ZD-I molecular models. The easiest chemical bonds breaking are almost related to oxygen atom, occurring in the C−O bond (consistent with the analysis of ESP analysis). And furthermore, aliphatic C−O is more prone to break than aromatic C−O (Tables S1 and S2). Compared with ZD-I, ZD-V has more easily broken bonds, further indicating that vitrinite is more reactive.

3.3. Adsorption Site Selection. Here, limited by quantum chemistry computing power, small molecular fragments of coal models located on the weaker bond on the edge of the molecule were selected to study the adsorption of Na^+ and Ca^{2+}. By focusing on small molecular fragments, we can
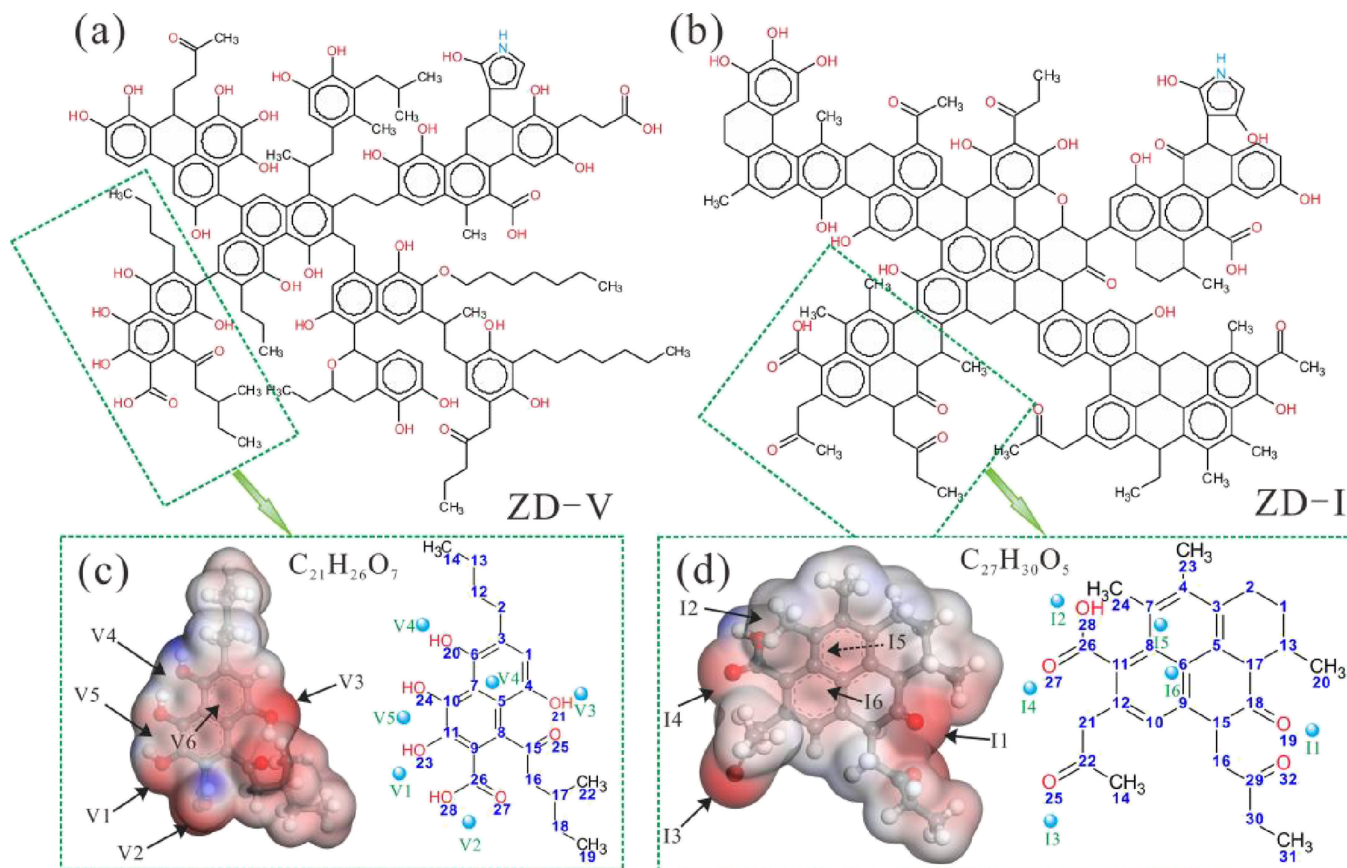
Figure 3. Selected molecular fragments from the ZD-V (a) and ZD-I (b) molecular structure model and its determined adsorption sites (c, d).
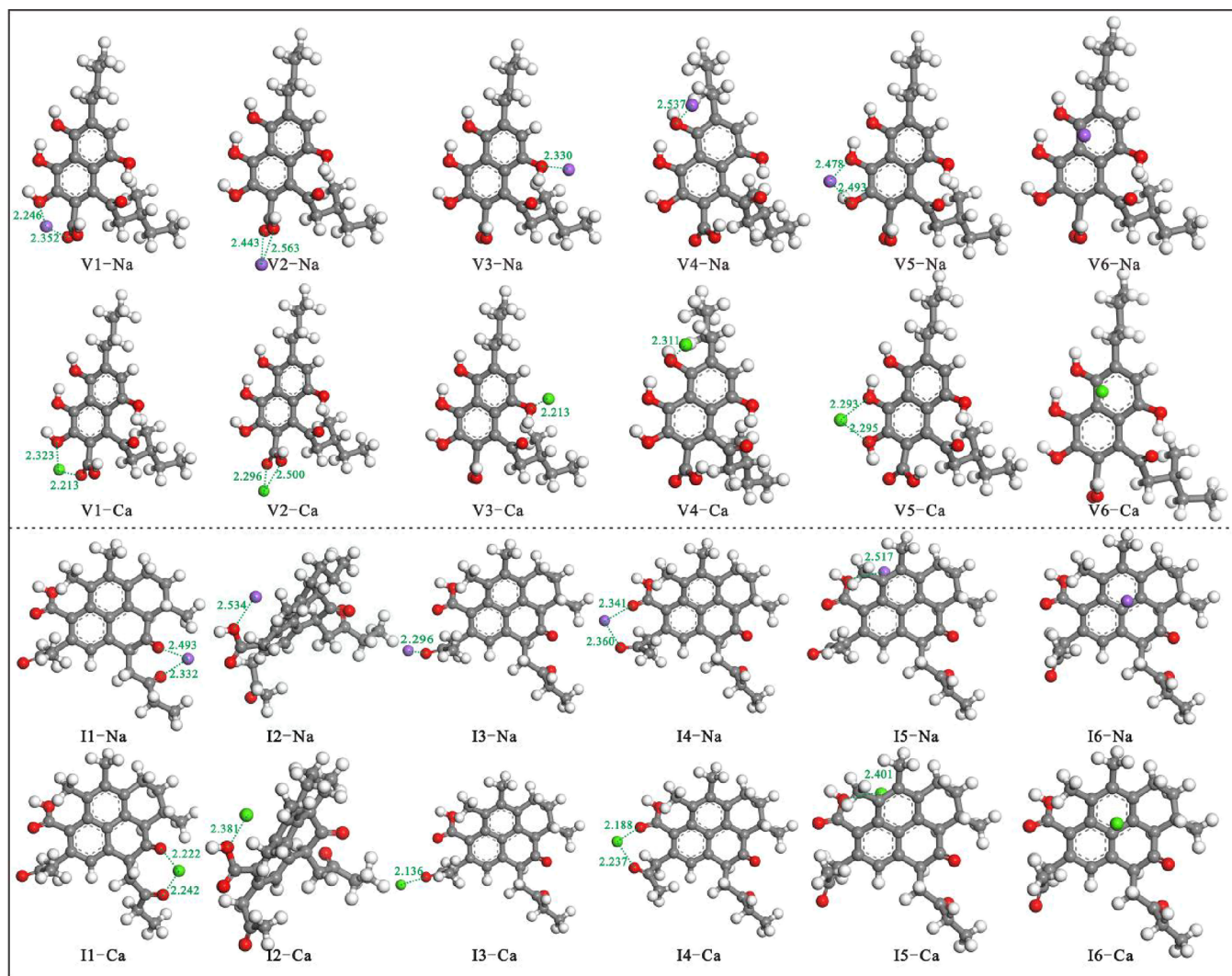
Figure 4. Molecular configuration for ZD-V and ZD-I molecular fragments separately at different sites after adsorption of Na$^+$ and Ca^{2+}.

avoid the influence of large molecular systems with cross-linked structures. Therefore, we selected molecule fragments of ZD-V and ZD-I with a chemical formula of $C_{21}H_{26}O_7$ and $C_{27}H_{30}O_5$, respectively, to determine the optimal adsorption site, as shown in Figure 3. First, the region with the highest red ESP near the oxygen-containing functional group was selected as the adsorption sites.[29] Additionally, adsorption sites near the aromatic ring were also chosen. The specific locations of the initial binding sites are labeled as V1, V2, V3, V4, V5, and V6 for the ZD-V molecular fragment as well as I1, I2, I3, I4, and I5 for the ZD-I molecular fragment, respectively (Figure 3). Specifically, for the ZD-V molecular fragment, V1 is near the hydroxyl and carboxyl groups, and V2 is positioned close to the two oxygen atoms within the carboxyl group. V3 and V4 can be perceived as primarily adjacent to the oxygen atom within a single hydroxyl group, whereas V5 is located between two hydroxyl groups. V6 is near the aromatic ring. For the ZD-I molecular fragment, I1 is located between two carboxyl groups, and I2 is closer to the single-bonded oxygen atom in the carboxyl group. I3 and I4 are close to the oxygen atom of the single carbonyl group. I5 and I6 are near the aromatic ring.

3.4. Adsorption AAEM Ions. Figure 4 shows the molecular configurations for ZD-V and ZD-I molecular fragments after the adsorption of Na$^+$ and Ca^{2+} at different

adsorption sites, respectively. It can be seen that after the adsorption of AAEM ions, the small molecule fragments undergo slight deformation and bending toward the adsorbed AAEM ions. For the ZD-V molecular fragments, the binding distance between O and Na ranges from 2.246 to 2.563 Å, whereas the binding distance between O and Ca ranges from 2.213 to 2.500 Å. The lowest binding distances occur at the adsorption site V1, where the oxygen atoms are concentrated, indicating that the AAEM ions can easily bind to the mixed oxygen-containing functional groups. In the case of the ZD-I molecular fragment, the binding distance between O and Na ranges from 2.296 to 2.534 Å, whereas the binding distance between O and Ca ranges from 2.136 to 2.318 Å. The lowest binding distances are all observed at the adsorption site I3, suggesting a preference for binding to oxygen in the C=O group. Furthermore, upon comparison of the difference between adsorbed Na$^+$ and Ca^{2+} at the same location, it is evident that Ca^{2+} bonds closer to O than adsorbed Na$^+$, indicating a greater affinity of Ca^{2+} for organic matter. Sequential extraction experiments have also revealed that water-soluble Ca was much less abundant than ion-exchanged Ca in Zhundong coal, whereas Na primarily occurred as water-soluble Na (Table 1). The occurrence of ion exchange implies that the ions have been bound to organic matter, further

confirming that Ca has a greater propensity to bind to organic matter than Na.

To further quantify the organic affinity of AAEM for Zhundong coal molecules, the adsorption energy between AAEM and organic small molecular fragments in different adsorption sites is calculated in Figure 5. The adsorption
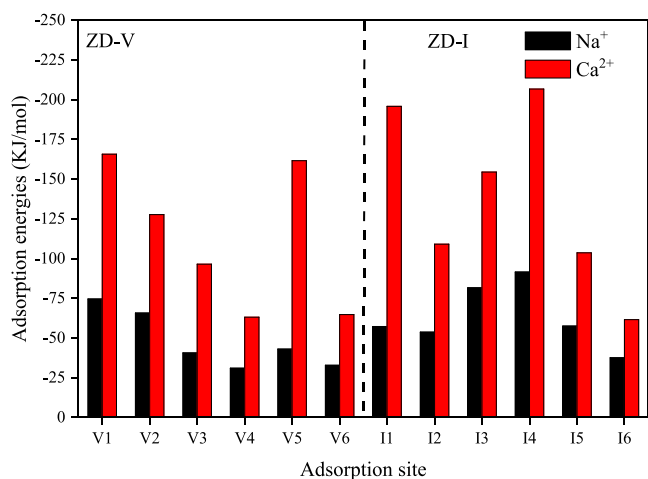

Figure 5. Adsorption energies of different adsorption sites in molecular fragments of ZD-V and ZD-I.

energies for all adsorption sites were negative, indicating that the reaction was exothermic and spontaneous.[41] Comparing the different AAEM ions, the adsorption energy of Ca^{2+} is nearly double that of Na^+ when it is adsorbed onto the same initial adsorption site, whether for ZD-V or ZD-I molecular fragments. This confirms that Ca^{2+} has a stronger affinity for organic matter in coal compared to Na^+. Taking Na^+ as an example, the maximum adsorption energy occurs at the V1 adsorption site in the molecular fragment of ZD-V followed by V2, V5, V3, V6, and V4 adsorption sites. The adsorption energy values were concentrated in the range of −31.049 to −74.569 kJ/mol. In the molecular fragment of ZD-I, the distribution of adsorption energy values (−37.589 to −91.556 kJ/mol) for Na^+ was slightly higher than that for the former. This indicates that Na^+ tends to bind to the carbonyl group, especially if multiple carbonyl groups are contained in the vicinity. When adsorption occurs near the aromatic ring,

different from the V5 and I6 adsorption sites, the AAEM adsorbed at I5 is attracted by the oxygen atom in the carboxyl group (constrained by the molecular configuration; Figure 3). The higher adsorption energy at I5 compared to V5 and I6 adsorption sites indicates that AAEM is more likely to bind with organic matter in the presence of oxygen. We also considered adsorption on the nitrogen atom of the heterocyclic pyrrole ring (Figure S2), and the adsorption occurs toward the direction away from nitrogen and closer to the oxygen atom.[42]

From the perspective of adsorption types, adsorption can be classified into physisorption and chemisorption based on the magnitude of adsorption energy. Chemisorption refers to strong attractive forces between the adsorbate and the sorbent, with adsorption energies ranging from 50 to 960 kJ/mol. Adsorption energies below 50 kJ/mol are classified as physisorption.[42] Here, Ca^{2+} in all adsorption sites is bound to organic molecules through chemisorption, exhibiting strong ionic force. Water molecules is hard to dissolve the Ca^{2+} adsorbed onto organic matter. This also reveals the reason for the low water-soluble Ca content in sequential extraction experiments (Table 1) insight from molecular perspective. Unlike Ca^{2+}, not all Na^+ species undergo chemisorption at every adsorption site. In addition to carbonyl and carboxyl groups, Na adsorbed alone to the hydroxyl group or near the aromatic ring is considered as physisorption. This is also the reason why Na primarily exists in water-soluble form in coal.

3.5. Effect of AAEM Ion Adsorption on the Nearby Atom Charge. The Mulliken charges were usually calculated to evaluate the partial atomic charges of heteroatoms in coal. Table 2 shows the calculated values of the nearby atomic charges and their differences before and after the adsorption of the AAEM ions. Before adsorption, the oxygen atom charges of the ZD-V and ZD-I molecular fragments were distributed between −0.416 to −0.540e and −0.424 to −0.472e, respectively. The relatively concentrated charge of oxygen atoms in the ZD-I molecular fragment is due to the fact that oxygen atoms exist mainly in the carbonyl form and the atomic charge is related to the forms of chemical bond existence.[22] When adsorption with AAEM ions occurs, it makes the charge of nearby oxygen atoms decrease, but the degree of decrease is different. For the ZD-V molecular fragment, the charge reduction caused by Na^+ ranges from 0.02 to 0.078e, whereas the reduction by Ca^{2+} reaches 0.083 to 0.161e. Similarly, for

Table 2. Calculated Values of Nearby Atomic Charges and Their Differences before and after the Adsorption of AAEM Ions

| molecular fragment	absorption site	nearby atom number	Mulliken charge			charge change	
			before absorption	after absorption Na^+	after absorption Ca^{2+}	after absorption Na^+	after absorption Ca^{2+}
ZD-V	V1	O23	−0.473	−0.514	−0.586	−0.041	−0.113
		O27	−0.416	−0.463	−0.561	−0.047	−0.145
	V2	O27	−0.416	−0.436	−0.499	−0.020	−0.083
	V3	O21	−0.532	−0.610	−0.682	−0.078	−0.150
	V4	O20	−0.540	−0.597	−0.640	−0.057	−0.100
	V5	O23	−0.473	−0.534	−0.634	−0.061	−0.161
		O24	−0.501	−0.528	−0.634	−0.027	−0.133
ZD-I	I1	O19	−0.433	−0.471	−0.552	−0.038	−0.119
		O32	−0.464	−0.507	−0.548	−0.043	−0.084
	I2	O28	−0.424	−0.462	−0.549	−0.038	−0.125
	I3	O25	−0.450	−0.483	−0.568	−0.033	−0.118
	I4	O25	−0.450	−0.478	−0.597	−0.028	−0.147
		O27	−0.472	−0.505	−0.532	−0.033	−0.060
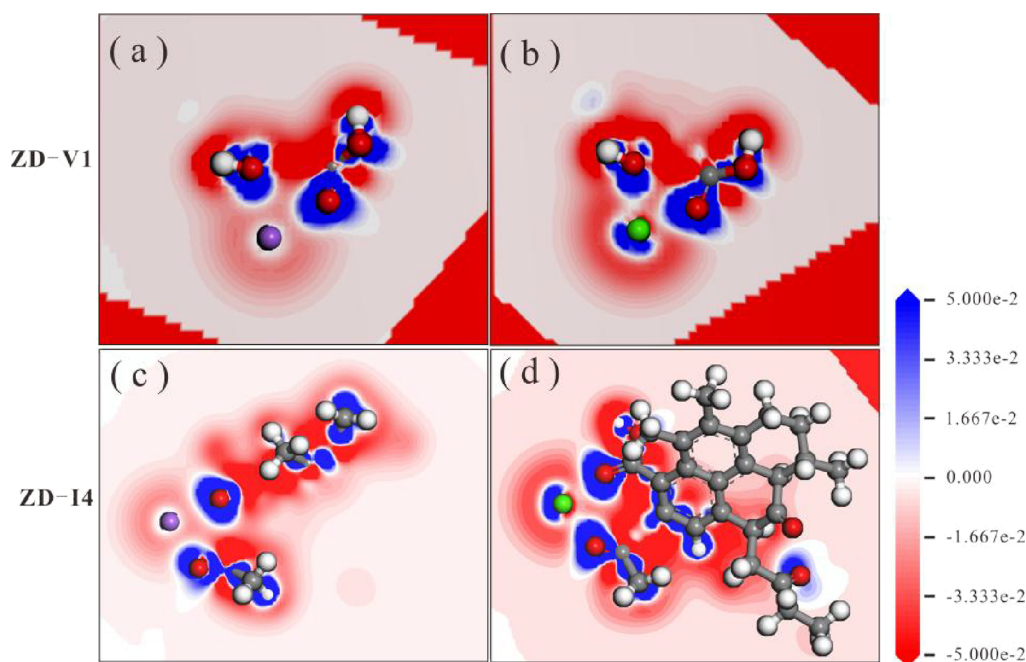
Figure 6. Deformation electron density of Na$^+$ and Ca^{2+} adsorption on ZD-V1 and ZD-I4 molecular fragment surface: (a) ZD-V1: Na$^+$; (b) ZD-V1: Ca^{2+}; (c) ZD-I4: Na$^+$; and (d) ZD-I4: Ca^{2+}.
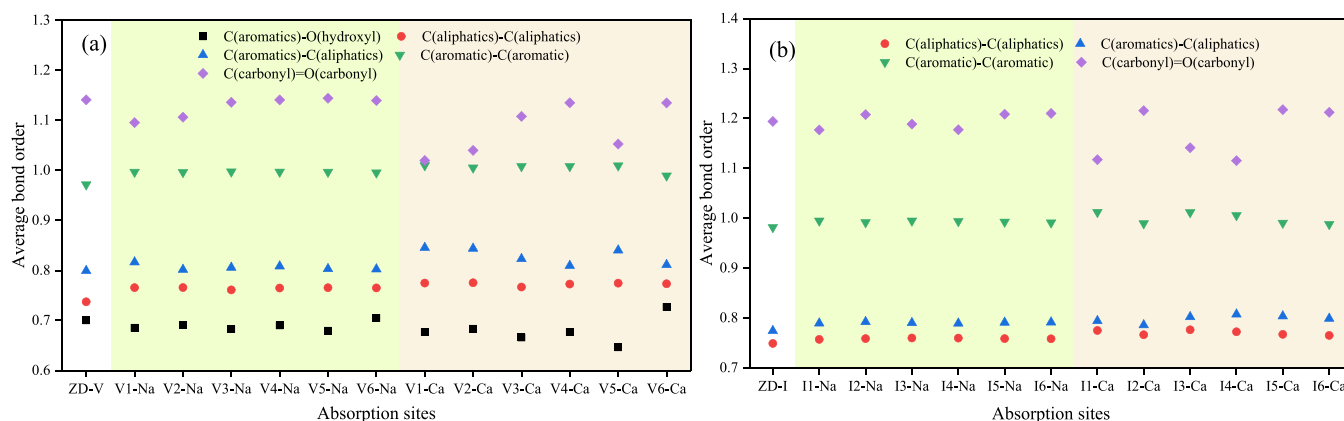

Figure 7. Average bond order for different chemical bond types of ZD-V (a) and ZD-I (b) molecular fragments in different sites after adsorption of AAEM ions.

the ZD-I molecular fragment, the charge reduction caused by Na$^+$ ranges from 0.028 to 0.043e, whereas the reduction by Ca^{2+} reaches 0.060 to 0.147e. All of these results indicate that the charge of oxygen atoms decreases more significantly after the adsorption of Ca^{2+} compared to Na$^+$. Therefore, the adsorption of AAEM ions causes charge transfer to the atoms in their vicinity, and more charge transfer indicates stronger binding to them.[43] From the adsorption of different AAEM ions at the same sites, the adsorption of Ca^{2+} resulted in more charge transfer from nearby atoms than that from Na$^+$, indicating a stronger binding of coal molecular fragments with Ca^{2+}. According to the previous studies on the radical reactions in organic matter,[22] the reactivity of heteroatom-containing groups is mainly controlled by the electronegativity and electron density of the heteroatoms. Thus, the adsorbed AAEM ions can make the chemical reactivity of nearby oxygen atoms increase based on Mulliken charge analysis.

To visualize the charge transfer, planar slices were created along the AAEM ions with two nearby adjacent oxygen atoms

at the optimal adsorption sites (ZD-V at V1 and ZD-I at I4) as an example. The deformation electron density of Na$^+$ and Ca^{2+} adsorption on the surface of the ZD-V and ZD-I molecular fragment was calculated, respectively (Figure 6). In Figure 6, red represents loss of electrons, whereas blue represents gain of electrons.[43] It can be observed that both Na$^+$ and Ca^{2+} lose charge, and the amount of charge can be rich on the oxygen atom in the ZD-V and ZD-I molecular fragments, which indicates that the charge exchange mainly occurred between the oxygen atom and substrate. Furthermore, electron transfer of Na$^+$ and Ca^{2+} mainly occurs along the direction of oxygen atoms. Compared to the electron transfer of Na$^+$, Ca^{2+} loses some electrons but gets parts of electrons. In addition, the number of lost electrons for Ca^{2+} is significantly higher than that of Na$^+$, indicating that Ca^{2+} could more easily bind with the coal molecule, which is in agreement with the result of the above analysis.

3.6. Effect of AAEM Ion Adsorption on the Chemical Bond of a Molecule. The bond order and bond length are

Table 3. Bond Order, Bond Length, and Their Change Values of Chemical Bonds in the Vicinity before and after Adsorption of AAEM Ions

molecular fragment	absorption sites	nearby chemical bonds	bond order			bond order change	
			before absorption	after absorption Na$^+$	after absorption Ca^{2+}	after absorption Na$^+$	after absorption Ca^{2+}
ZD-V	V1	C11−O23 (hydroxyl)	0.741	0.646	0.545	−0.095	−0.196
		C26−O27 (carbonyl)	1.265	1.173	1.020	−0.092	−0.246
	V2	C26−O27 (carbonyl)	1.265	1.197	1.067	−0.068	−0.198
	V3	C4−O21 (hydroxyl)	0.704	0.639	0.504	−0.065	−0.200
	V4	C6−O20 (hydroxyl)	0.606	0.529	0.420	−0.077	−0.186
	V5	C11−O23 (hydroxyl)	0.741	0.651	0.579	−0.090	−0.162
		C10−O24 (hydroxyl)	0.705	0.671	0.570	−0.034	−0.136
ZD-I	I1	C18−O19 (carbonyl)	1.211	1.169	1.041	−0.042	−0.169
		C29−O32 (carbonyl)	1.182	1.133	1.014	−0.050	−0.168
	I2	C26−O28 (hydroxyl)	0.771	0.725	0.751	−0.047	−0.020
	I3	C22−O25 (carbonyl)	1.163	1.105	0.949	−0.058	−0.214
	I4	C22−O25 (carbonyl)	1.163	1.115	1.011	−0.049	−0.152
		C26−O27 (carbonyl)	1.219	1.202	1.036	−0.017	−0.183
			bond length/Å			bond length change/Å	
ZD-V	V1	C11−O23 (hydroxyl)	1.365	1.376	1.394	0.011	0.029
		C26−O27 (carbonyl)	1.213	1.229	1.249	0.016	0.036
	V2	C26−O27 (carbonyl)	1.213	1.227	1.247	0.014	0.034
	V3	C4−O21 (hydroxyl)	1.358	1.382	1.396	0.024	0.038
	V4	C6−O20 (hydroxyl)	1.406	1.416	1.433	0.010	0.027
	V5	C11−O23 (hydroxyl)	1.365	1.388	1.378	0.023	0.013
		C10−O24 (hydroxyl)	1.366	1.364	1.378	−0.002	0.012
ZD-I	I1	C18−O19 (carbonyl)	1.230	1.235	1.246	0.005	0.016
		C29−O32 (carbonyl)	1.235	1.242	1.251	0.007	0.016
	I2	C26−O28 (hydroxyl)	1.361	1.374	1.406	0.013	0.045
	I3	C22−O25 (carbonyl)	1.234	1.239	1.254	0.005	0.020
	I4	C22−O25 (carbonyl)	1.234	1.238	1.249	0.004	0.015
		C26−O27 (carbonyl)	1.233	1.237	1.255	0.004	0.022

physical quantities that describe the strength of bonding between adjacent atoms in a molecule and help to determine the active site in the molecular structure of coal where cracking occurs. These parameters are indicators of the strength of the chemical bonds. Generally, the smaller the bond order or the larger the bond length is, the more unstable and reactive the state is, and the more easily the chemical bond breaks.[20,44] Figure 7 shows the effect of different sites on the average bond order for various types of chemical bonds in ZD-V and ZD-I molecular fragments after the adsorption of AAEM ions. The AAEM ions cause a slight increase in the bond order of chemical bonds containing carbon−carbon and a decrease in the bond order of chemical bonds containing carbon−oxygen

in general terms. When adsorption of AAEM ions occurs, the average bond order of C(aromatics)−O(hydroxyl) of ZD-V molecular fragments decreases significantly, indicating that AAEM ions have a shearing effect on the hydroxyl group. The average bond order of C(carbonyl)═O(carbonyl) exhibits a wide variation range across different adsorption sites. AAEM ions at V1, V2, I1, I3, and I4 sites (near the carbonyl) cause a reduction in average bond order of the C(carbonyl)═O(carbonyl). Moreover, compared to Na$^+$, Ca^{2+} makes the average bond order of C(carbonyl)═O(carbonyl) decrease more significantly.

Table 3 shows the detailed bond order, bond length, and change values of chemical bonds in the vicinity before and after
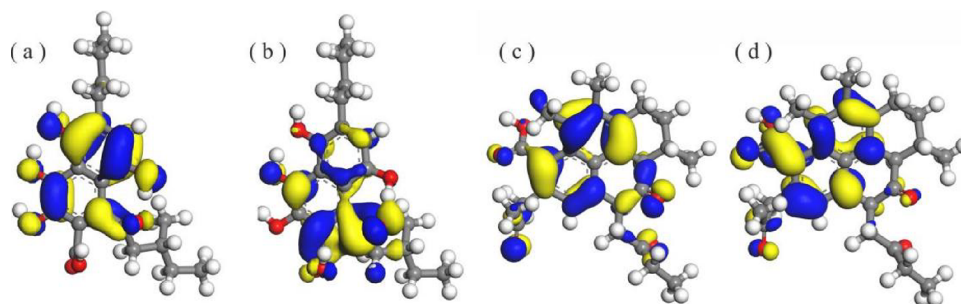
Figure 8. Molecular orbital map of HOMO and LUMO for the ZD-V and ZD-I molecular fragment. ZD-V: (a) HOMO and (b) LUMO; ZD-I: (c) HOMO and (d) LUMO.
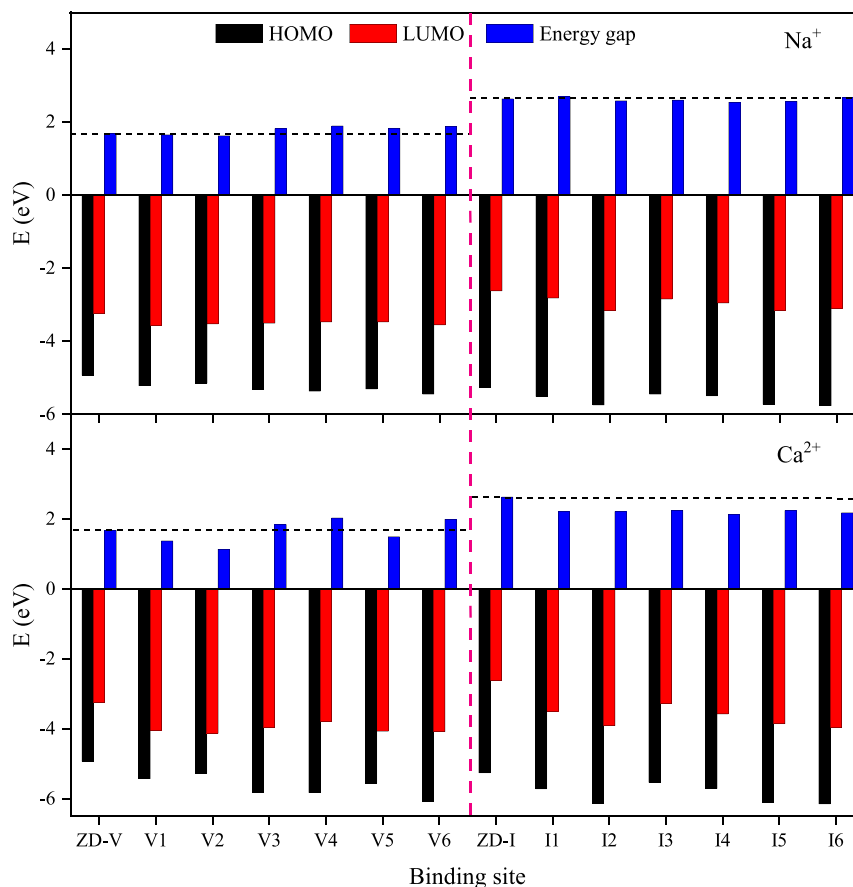

Figure 9. Molecular orbital analysis for molecular fragments of ZD-V and ZD-I and after their absorption of AAEM ions.

the adsorption of AAEM ions, and the results conclude that the adsorption of AAEM ions exerts a major effect on the chemical bonds of oxygen-containing functional groups near the molecular fragments. The oxygen-containing functional groups near the ZD-V molecular fragment are mainly composed of hydroxyl groups, whereas ZD-I is dominated by carbonyl groups. The hydroxyl group (C−O) has a bond order of 0.606−0.771 and a bond length between 1.358 and 1.406 Å, whereas the carbonyl group (C=O) has a larger bond order (1.163−1.265) and a smaller bond length (1.213−1.235 Å). After the adsorption of Na^+ with the ZD-I molecular fragment, the bond order decreased by 0.017−0.058 Å, and the bond length increased by 0.004−0.013 Å. And after adsorption of Na^+ by the ZD-V molecular fragment, the bond order decreased by 0.065−0.096 Å, and the bond length increased by 0.010−0.024 Å, indicating a slightly greater effect than that

of ZD-I. The effect of Na^+ was smaller on the carbonyl group but slightly greater on the nearby hydroxyl group. Almost all other adjacent adsorption sites showed a trend of decreasing bond order and increasing bond length (Table 3). Compared to Na^+, the adsorption of Ca^{2+} resulted in a greater reduction of the bond order (except for the I2 site) and a greater increase in bond length, making the chemical bonds more easily break. Therefore, the adsorption of AAEM ions plays an important role in oxygen removal during the coal pyrolysis reactions. The AAEM ions in coal make the hydroxyl group more prone to break up during the pyrolysis reaction, leading to increased water yields. These insights also suggest that the adsorbed AAEM ions have a more significant effect on the chemical bond of oxygen-containing functional groups near AAEM ions compared to the overall molecular fragments.

3.7. Effect of AAEM Ion Adsorption on the Molecular Orbital. Frontier orbitals, including the highest occupied molecular orbital (HOMO) and the lowest unoccupied molecular orbital (LUMO), often play dominant roles in the chemical reactions of a molecular system.[22,45] The electrons in HOMO are usually easy to lose, whereas the LUMO prefers to accept electrons.[46] The HOMO and LUMO molecular orbitals of ZD-V and ZD-I are mainly concentrated in the naphthalene ring and its adjacent side chain (Figure 8). The atom for the molecular edge contributes little to the HOMO and LUMO molecular orbitals. Here, to evaluate the effect of Na$^+$ and Ca^{2+} adsorption on the molecular orbital of coal, the HOMO energy (E_{HOMO}), LUMO energy (E_{LUMO}), and energy gaps ($\Delta E_{gap} = E_{HOMO} - E_{LUMO}$) were calculated for ZD-V and ZD-I molecular fragments both before and after adsorption of Na$^+$/Ca^{2+} at different sites, as shown in Figure 9. Where ΔE_{gap} can describe the reactivity of the molecule, the narrower the energy gap of the molecule is, the more active the reaction is.[47,48] The ΔE_{gap} of the ZD-V molecular fragment was 1.686 eV, which was smaller than the 2.637 eV of the ZD-I fragment, indicating that the ZD-V molecular fragment has a higher reactivity. The energy levels of both HOMO and LUMO orbitals decreased after the adsorption of AAEM ions, but the degree of decrease was different. Whether for the ZD-V or ZD-I molecular fragment, the degree of decrease after the adsorption of Na$^+$ was significantly smaller than that of Ca^{2+}, indicating that Ca^{2+} has a more significant effect on the molecular orbitals. Also, the adsorbed AAEM ions affected ΔE_{gap} to different degrees, with a slight effect on ΔE_{gap} after the adsorption of Na$^+$ and a more significant effect after the adsorption of Ca^{2+}. After adsorption of Ca^{2+}, ΔE_{gap} significantly decreased at all sites except for V3, V4, and V6. That is, apart from AAEM ions adsorbed near the hydroxyl group and aromatic ring alone, other adsorption sites make the chemical reaction easy to occur and are particularly conducive to nucleophilic or electrophilic reactions. It should be noted that although the I5 and I6 adsorption sites is also near the aromatic ring, it may be affected by carboxyl and carbonyl group when adsorption occurs, and thus, ΔE_{gap} is reduced.

The speculation here is that ΔE_{gap} is related to the adsorption capacity. When AAEM ions undergo physisorption with organic molecular fragments, the interaction between them is primarily caused by van der Waals forces. Physisorption does not significantly alter the electron structure of the molecules, resulting in ΔE_{gap} stabilization. However, during chemisorption, stronger interactions are formed between the organic molecular fragments and the AAEM ions. This provides more reaction sites and pathways for electron transfer. Consequently, chemisorption is more likely to induce nucleophilic or electrophilic reactions.

4. CONCLUSIONS

In this study, the optimal adsorption sites of Na$^+$ and Ca^{2+} on Zhundong coal molecules were determined by adsorption distance, adsorption energy, and ESP. The effect of the adsorption of Na$^+$ and Ca^{2+} at different adsorption sites on the electronic properties of coal molecular fragments, including atomic charges, chemical bonds, and molecular orbitals, was investigated from a quantum chemical perspective. Detailed conclusions are as follows:

1 Compared to ZD-I, ZD-V exhibits a higher distribution of negative potential and smaller bond order, indicating

that vitrinite contains more adsorption sites for AAEM ions and exhibits stronger chemical reactivity. This is primarily attributed to the abundance of oxygen-containing functional groups in vitrinite.

2 AAEM ions are easily adsorbed near the oxygen-containing functional groups in coal. The optimal adsorption site occurs at the V1 and I4 where there are mixed oxygen-containing functional groups nearby, whereas if only a single oxygen-containing functional group is present in the vicinity of AAEM ions, the optimal adsorption site occurs near the carbonyl group (C=O). Compared with the adsorption of Na$^+$, Ca^{2+} has a smaller adsorption distance from the molecule and a higher adsorption energy. Ca^{2+} has the ability to transfer more charge than Na$^+$ and exhibits a stronger affinity with coal molecules.

3 Adsorption of AAEM ions has a greater impact on the chemical bond of oxygen-containing functional groups near these ions compared to the overall molecular fragments. This leads to a decrease in bond order and an increase in bond length of the nearby oxygen-containing functional groups. Compared with the adsorption of Na$^+$, Ca^{2+} makes the nearby chemical bonds more prone to break.

4 Ca^{2+} at all adsorption sites is bound to organic molecules by chemisorption, which also reveals the reason for the low water-soluble Ca content in coal from the molecular point of view. Na$^+$ binds to organic molecules by chemisorption when in the vicinity of the carbonyl or carboxyl group, and physisorption occurs when Na$^+$ approaches the hydroxyl or aromatic ring alone. Compared with the adsorption of Na$^+$, Ca^{2+} has a more significant effect on ΔE_{gap}. The adsorption of Ca^{2+} near carbonyl and carboxyl groups leads to a significant decrease in ΔE_{gap}, indicating an enhanced chemical reactivity of coal molecular fragments.

■ ASSOCIATED CONTENT

ⓈI Supporting Information

The Supporting Information is available free of charge at https://pubs.acs.org/doi/10.1021/acsomega.3c04985.

Easiest breaking place of chemical bonds (Figure S1); bond order parameters (Tables S1 and S2); and changes in the spatial configuration of AEEM ions absorbed on the nitrogen atom of the heterocyclic pyrrole ring (Figure S2) (PDF)

■ AUTHOR INFORMATION

Corresponding Author

Shaoqing Wang — College of Geoscience and Surveying Engineering, China University of Mining and Technology (Beijing), Beijing 100083, China; ● orcid.org/0000-0001-5158-7751; Phone: +86 10 6233-1657; Email: wangzq@cumtb.edu.cn

Authors

Xiaoling Wang — College of Geoscience and Surveying Engineering, China University of Mining and Technology (Beijing), Beijing 100083, China

Yungang Zhao — College of Geoscience and Surveying Engineering, China University of Mining and Technology (Beijing), Beijing 100083, China

Ruifeng Mu − *College of Geoscience and Surveying Engineering, China University of Mining and Technology (Beijing), Beijing 100083, China*

Yan Shao − *College of Geoscience and Surveying Engineering, China University of Mining and Technology (Beijing), Beijing 100083, China*

Notes

The authors declare no competing financial interest.

■ REFERENCES

(1) Zhou, J.; Zhuang, X.; Alastuey, A.; Querol, X.; Li, J. Geochemistry and mineralogy of coal in the recently explored Zhundong large coal field in the Junggar basin, Xinjiang province, China. *International Journal of Coal Geology* **2010**, *82*, 51−67.

(2) Zhu, C.; Qu, S.; Zhang, J.; Wang, Y.; Zhang, Y. Distribution, occurrence and leaching dynamic behavior of sodium in Zhundong coal. *Fuel* **2017**, *190*, 189−197.

(3) Yu, J.; Ding, L.; Cheng, C.; Mosqueda, A.; Bai, Y.; Yu, G. Release characteristics of alkali and alkaline earth metals in nascent char during rapid pyrolysis. *Fuel* **2022**, *323*, No. 124376.

(4) Durie, R. A. *The Science of Victorian Brown Coal: Structure, Properties and Consequences for Utilisation.* Butterworth-Heinemann: Oxford, UK, 1991 DOI: 10.1016/C2013-0-04527-6.

(5) Li, C. Z.; Sathe, C.; Kershaw, J. R.; Pang, Y. Fates and roles of alkali and alkaline earth metals during the pyrolysis of a Victorian brown coal. *Fuel* **2000**, *79*, 427−438.

(6) Li, W.; Wang, L.; Qiao, Y.; Lin, J.; Wang, M.; Chang, L. Effect of atmosphere on the release behavior of alkali and alkaline earth metals during coal oxy-fuel combustion. *Fuel* **2015**, *139*, 164−170.

(7) Shi, H.; Wu, Y.; Zhang, M.; Zhang, Y.; Lyu, J. Ash deposition of Zhundong coal in a 350 MW pulverized coal furnace: Influence of sulfation. *Fuel* **2020**, *260*, No. 116317.

(8) Reinmöller, M.; Schreiner, M.; Guhl, S.; Neuroth, M.; Meyer, B. Ash behavior of various fuels: The role of the intrinsic distribution of ash species. *Fuel* **2019**, *253*, 930−940.

(9) Abdalazeez, A.; Li, T.; Wang, W.; Abuelgasim, S. A brief review of CO_2 utilization for alkali carbonate gasification and biomass/coal co-gasification: Reactivity, products and process. *Journal of CO_2 Util.* **2021**, *43*, No. 101370.

(10) Sadhwani, N.; Adhikari, S.; Eden, M. R.; Wang, Z.; Baker, R. Southern pines char gasification with CO_2—Kinetics and effect of alkali and alkaline earth metals. *Fuel Process. Technol.* **2016**, *150*, 64−70.

(11) Kawashima, H.; Takanohashi, T. Modification of model structures of Upper Freeport coal extracts using ^{13}C-NMR chemical shift calculations. *Energy Fuels* **2001**, *15*, 591−598.

(12) Erdenetsogt, B.; Lee, I.; Lee, S. K.; Ko, Y.; Bat-Erdene, D. Solid-state C-13 CP/MAS NMR study of Baganuur coal, Mongolia: Oxygen-loss during coalification from lignite to subbituminous rank. *International Journal of Coal Geology* **2010**, *82*, 37−44.

(13) He, X.; Liu, X.; Nie, B.; Song, D. FTIR and Raman spectroscopy characterization of functional groups in various rank coals. *Fuel* **2017**, *206*, 555−563.

(14) Jiang, J.; Yang, W.; Cheng, Y.; Liu, Z.; Zhang, Q.; Zhao, K. Molecular structure characterization of middle-high rank coal via XRD, Raman and FTIR spectroscopy: Implications for coalification. *Fuel* **2019**, *239*, 559−572.

(15) Wang, J.; He, Y.; Li, H.; Yu, J.; Xie, W.; Wei, H. The molecular structure of Inner Mongolia lignite utilizing XRD, solid state ^{13}C NMR, HRTEM and XPS techniques. *Fuel* **2017**, *203*, 764−773.

(16) Zhong, Q.; Mao, Q.; Zhang, L.; Xiang, J.; Xiao, J.; Mathews, J. P. Structural features of Qingdao petroleum coke from HRTEM lattice fringes: Distributions of length, orientation, stacking, curvature, and a large-scale image-guided 3D atomistic representation. *Carbon* **2018**, *129*, 790−802.

(17) Wang, X.; Wang, S.; Hao, C.; Zhao, Y.; Song, X. Quantifying orientation and curvature in HRTEM lattice fringe micrographs of naturally thermally altered coals: New insights from a structural evolution perspective. *Fuel* **2022**, *309*, No. 122180.

(18) Wu, B.; Hu, H.; Zhao, Y.; Jin, L.; Fang, Y. XPS analysis and combustibility of residues from two coals extraction with sub- and supercritical water. *Journal of Fuel Chemistry and Technology* **2009**, *37*, 385−392.

(19) Wang, C.; Zeng, F. Molecular Structure Characterization of CS_2-NMP Extract and Residue for Malan Bituminous Coal via Solid-State ^{13}C NMR, FTIR, XPS, XRD, and CAMD Techniques. *Energy Fuels* **2020**, *34*, 12142−12157.

(20) Wang, Y.; Lian, J.; Xue, Y.; Liu, P.; Dai, B.; Lin, H.; Han, S. The pyrolysis of vitrinite and inertinite by a combination of quantum chemistry calculation and thermogravimetry-mass spectrometry. *Fuel* **2020**, *264*, No. 116794.

(21) Zhao, Y.; Wang, S.; Liu, Y.; Song, X.; Chen, H.; Zhang, X.; Lin, Y.; Wang, X. Molecular modeling and reactivity of thermally altered coals by molecular simulation techniques. *Energy Fuels* **2021**, *35*, 15663−15674.

(22) Pan, S.; Wang, Q.; Bai, J.; Chi, M.; Cui, D.; Wang, Z.; Liu, Q.; Xu, F. Molecular structure and electronic properties of oil shale kerogen: An experimental and molecular modeling study. *Energy Fuels* **2018**, *32*, 12394−12404.

(23) Zhang, J.; Han, C. L.; Yan, Z.; Liu, K.; Xu, Y.; Sheng, C. D.; Pan, W. P. The varying characterization of alkali metals (Na, K) from coal during the initial stage of coal combustion. *Energy Fuels* **2001**, *15*, 786−793.

(24) Bai, X.; Wang, Y.; Ding, H.; Zhu, C.; Zhang, Y. Modes of occurrence of sodium in Zhundong coal. *J. China Coal Soc.* **2015**, *40*, 2909−2915.

(25) Yang, Y.; Wu, Y.; Zhang, H.; Zhang, M.; Liu, Q.; Yang, H.; Lu, J. Improved sequential extraction method for determination of alkali and alkaline earth metals in Zhundong coals. *Fuel* **2016**, *181*, 951−957.

(26) Yang, X.; Lv, P.; Zhu, S.; Yan, L.; Bai, Y.; Li, F. Release of Ca during coal pyrolysis and char gasification in H_2O, CO_2 and their mixtures. *Journal of Analytical and Applied Pyrolysis* **2018**, *132*, 217−224.

(27) Wang, C.; Zhao, L.; Han, T.; Chen, W.; Yan, Y.; Jin, X.; Che, D. Release and transformation behaviors of sodium, calcium, and iron during oxy-fuel combustion of Zhundong Coals. *Energy Fuels* **2018**, *32*, 1242−1254.

(28) Hong, D.; Cao, Z.; Guo, X. Effect of calcium on the secondary reactions of tar from Zhundong coal pyrolysis: A molecular dynamics simulation using ReaxFF. *Journal of Analytical and Applied Pyrolysis* **2019**, *137*, 246−252.

(29) Sun, C.; Wei, X.; Kang, R.; Bin, F.; Li, S. Intrinsic sodium occurrence in Zhundong coal: Experimental observations and molecular modeling. *Fuel* **2021**, *305*, No. 121491.

(30) He, H.; Xing, L.; Zhang, J.; Tang, M. Binding characteristics of Cd^{2+}, Zn^{2+}, Cu^{2+}, and Li^+ with humic substances: Implication to trace element enrichment in low-rank coals. *Energy Exploration & Exploitation* **2016**, *34*, 735−745.

(31) Jeong, K.; Jeong, H. J.; Lee, G.; Kim, S. H.; Kim, K. H.; Yoo, C. G. Catalytic effect of alkali and alkaline earth metals in lignin pyrolysis: A density functional theory study. *Energy Fuels* **2020**, *34*, 9734−9740.

(32) Dai, S.; Hower, J. C.; Finkelman, R. B.; Graham, I. T.; French, D.; Ward, C. R.; Eskenazy, G.; Wei, Q.; Zhao, L. Organic associations

of non-mineral elements in coal: A review. *International Journal of Coal Geology* **2020**, *218*, No. 103347.

(33) Wang, X.; Wang, S.; Zhao, Y.; Liu, Y. Construction and verification of vitrinite-rich and inertinite-rich Zhundong coal models at the aggregate level: new insights from the spatial arrangement and thermal behavior perspective. *RSC Adv.* **2023**, *12*, 7569.

(34) Perdew, J.; Burke, K.; Ernzerhof, M. Generalized gradient approximation made simple. *Phys. Rev. Lett.* **1997**, *78*, 1396.

(35) Grimme, S. Semiempirical GGA-type density functional constructed with a long-range dispersion correction. *J. Comput. Chem.* **2006**, *27*, 1787−1799.

(36) Thul, P.; Gupta, V. P.; Ram, V. J.; Tandon, P. Structural and spectroscopic studies on 2-pyranones. *Spectrochimica Acta Part A: Molecular and Biomolecular Spectroscopy* **2010**, *75*, 251−260.

(37) Murray, J. S.; Politzer, P. The electrostatic potential: an overview. *WIREs Computational Molecular Science* **2011**, *1*, 153−163.

(38) Lu, T.; Manzetti, S. Wavefunction and reactivity study of benzo[a]pyrene diol epoxide and its enantiomeric forms. *Structural Chemistry* **2014**, *25*, 1521−1533.

(39) Van Niekerk, D.; Pugmire, R. J.; Solum, M. S.; Painter, P. C.; Mathews, J. P. Structural characterization of vitrinite-rich and inertinite-rich Permian-aged South African bituminous coals. *International Journal of Coal Geology* **2008**, *76* (4), 290−300.

(40) Jin, L.; Han, K.; Wang, J.; Hu, H. Direct liquefaction behaviors of Bulianta coal and its macerals. *Fuel Process. Technol.* **2014**, *128*, 232−237.

(41) Mu, R.; Wang, S.; Wang, X.; Zhao, Y.; Dong, Z. Occurrence modes of critical metals (Li^+ and Ge^{4+}) in the organic molecular structures of coal: A density functional theory study. *ACS Omega* **2023**, *8*, 17264−17273.

(42) Xin, G.; Zhao, P.; Zheng, C. Theoretical study of different speciation of mercury adsorption on CaO (001) surface. *Proceedings of the Combustion Institute* **2009**, *32*, 2693−2699.

(43) Wang, Y.; Jin, J.; Kou, X.; Hou, F. Understanding the mechanism for the formation of initial deposition burning Zhundong coal: DFT calculation and experimental study. *Fuel* **2020**, *269*, No. 117045.

(44) Feng, J.; Li, J.; Li, W. Influences of chemical structure and physical properties of coal macerals on coal liquefaction by quantum chemistry calculation. *Fuel Process. Technol.* **2013**, *109*, 19−26.

(45) Wang, Q.; Pan, S.; Bai, J.; Chi, M.; Cui, D.; Wang, Z.; Liu, Q.; Xu, F. Experimental and dynamics simulation studies of the molecular modeling and reactivity of the Yaojie oil shale kerogen. *Fuel* **2018**, *230*, 319−330.

(46) Huo, Y.; Zhu, H.; He, X.; Fang, S.; Wang, W. Quantum chemistry calculation study on chain reaction mechanisms and thermodynamic characteristics of coal spontaneous combustion at low temperatures. *ACS Omega* **2021**, *6*, 30841−30855.

(47) Ruiz-Morales, Y. Application of the Y-rule and theoretical study to understand the topological and electronic structures of polycyclic aromatic hydrocarbons from atomic force microscopy images of soot, coal asphaltenes, and petroleum asphaltenes. *Energy Fuels* **2022**, *36*, 8725−8748.

(48) Wang, C.; Xing, Y.; Xia, Y.; Chen, P.; Chen, W.; Tan, J.; Zhang, C.; Gui, X. Effect of vacancy defects on electronic properties and wettability of coal surface. *Appl. Surf. Sci.* **2020**, *511*, No. 145546.